Mon. Not. R. Astron. Soc. **270**, 46–64 (1994)

Radio-continuum observations of the central regions of Sérsic–Pastoriza galaxies

D. J. Saikia,[1,2] A. Pedlar,[1] S. W. Unger[3] and D. J. Axon[4]

[1] *Nuffield Radio Astronomy Laboratories, Jodrell Bank, Macclesfield, Cheshire SK11 9DL*
[2] *National Centre for Radio Astrophysics, TIFR, Post Bag 3, Ganeshkhind, Pune 411 007, India*
[3] *Royal Greenwich Observatory, Madingley Road, Cambridge CB3 0EZ*
[4] *Space Telescope Science Institute, 3700 San Martin Drive, Baltimore, Maryland, USA*

Accepted 1994 March 28. Received 1993 November 4

ABSTRACT

We present radio-continuum observations, made with the VLA A-array at 20 cm and with the B-array at 6 cm, of a sample of 47 Sérsic–Pastoriza galaxies, 27 of which were detected. Those with a bright nucleus and well-defined hotspots in the central region at optical wavelengths are the most likely to be detected in this way. The radio emission often originates in compact components, most of which are likely to be supernova remnants (SNRs) occurring in regions of high star formation rate. The luminosities of these features range from $\sim 10^{18.5}$ to 10^{21} W Hz^{-1} at 6 cm, which is significantly higher than SNRs in our own Galaxy as well as those in M82. In a number of sources we find evidence of a ring or spiral-like pattern in the nuclear region at radio wavelengths. We discuss the possible origin of such structures, and attempt to identify those galaxies that are likely to have an active galactic nucleus (AGN).

Key words: galaxies: Seyfert – galaxies: starburst – radio continuum: galaxies.

1 INTRODUCTION

One of the important aspects of the study of activity in galaxies is to understand the physical conditions that might lead to either the formation of an active galactic nucleus (AGN) or an intense burst of star formation in the central regions. There have been many investigations exploring possible relationships between galaxy interactions, circumnuclear starbursts and the possible creation of a massive black hole as the end product of stellar evolution (Weedman 1983; Norman & Scoville 1988; Heckman 1990, 1992). Although there have been suggestions linking galaxy interactions to both starburst and AGN phenomena (cf. Heckman 1991), the conditions that might lead to the formation of an AGN are not well understood.

In recent years, attention has been focused on the *IRAS* galaxies with high ($10^{11} \leq L_{\rm FIR} \leq 10^{12}\,{\rm L}_{\odot}$) and ultrahigh ($L_{\rm FIR} \geq 10^{12}\,{\rm L}_{\odot}$) luminosities in the far-infrared region. Radio and far-infrared observations provide the most reliable way to study the nuclear regions of these sources, which are embedded in dust and are opaque at all but these long wavelengths. These observations have helped to develop diagnostics as to whether the bulk of the observed emission is due to an AGN or a starburst in the central region. Compact nuclear components whose brightness temperature exceeds about 10^{10} K or those that have well-collimated jets as in Mrk 3 (Kukula et al. 1993) are likely to be due to a supermassive black hole or AGN. However, since such signatures are often not available, the nature of the compact sources of emission is not always clear. Sopp & Alexander (1991) suggested that almost all the observed radio and far-infrared emission from the infrared-luminous galaxies is due to a starburst and not an active nucleus. They also showed that the ultraluminous infrared galaxies fit the FIR–radio relationship for normal star-forming galaxies. Norris et al. (1990) suggested that some with Seyfert-like optical spectra could be powered by supermassive black holes, while others could be due to starbursts. Condon et al. (1991) observed a large sample with the VLA and, assuming that their spectra could be flattened at 20 cm due to free–free absorption, showed that almost all of them could be explained by compact starbursts in the nuclear regions. Only one galaxy, namely Mrk 231, did not fit the FIR–radio relationship (Helou, Soifer & Rowan-Robinson 1985) and is likely to be due to a supermassive object or AGN; Neff & Ulvestad (1988) reported that the radio source is variable, with about 10–20 per cent variations over a period of a few months. Colina & Perez-Olea (1992) arrived at similar conclusions from a detailed study of a sample of high-luminosity and ultraluminous infrared galaxies.

To investigate some of the questions mentioned earlier, we started a project to study the properties of a sample of galaxies with morphologically peculiar nuclei. The definition of such a galaxy as one which exhibits a change in the slope of the luminosity profile and evidence of some structure (Sérsic & Pastoriza 1965; Sérsic 1973) includes galaxies with diffuse and amorphous nuclei, in addition to the well-known hotspot systems. These galaxies, which have been christened Sérsic–Pastoriza or S–P galaxies (Osmer, Smith & Weedman 1974), reflect a broad spectrum of properties, with some of them also harbouring a Seyfert nucleus. The existence of both starburst and Seyfert activity makes it of particular interest to study their kinematics, evolution and possible relationships between the two forms of activity. In an earlier paper, we reported radio-continuum, optical and H I observations of one of the galaxies in our sample, NGC 1808, where we discovered a family of compact radio sources which are likely to be compact SNRs (Saikia et al. 1990). In this paper, we now present radio observations of a sample of 47 galaxies which were made with the VLA at 20 and 6 cm, and discuss some of the possible implications of the results. A more detailed comparison with data at other wavebands will be presented later.

2 THE SAMPLE

The sources in our sample were selected almost entirely from those catalogued by Sérsic & Pastoriza (1965) and Sérsic (1973), or from the sample studied by Prabhu (1980) at optical wavelengths. They are listed in Table 1, which is

Table 1. The sample of Sérsic–Pastoriza galaxies.

Galaxy	Galaxy morph.		Nuclear morph.		$B_T^{0,i}$	V	D	maj.	min.	PA	Refs.
NGC	RSA	RC3	Sérsic	Prabhu		km s^{-1}	Mpc	′	′	°	
0210	Sb(rs)I	.SXS3..	AN	ϵ	11.01	1875	25.00	5.0	3.3	160	RC3
0255	SBc(r)II.3	.SXT4..	HS	$\sigma\iota$	12.03	1726	23.01	3.0	2.5	15	RC3
0613	SBb(rs)II	.SBT4..	HS	σ	10.19	1534	20.45	7.0	5.5	120	L82
0922	Sc(s)II.2 pec	.SBS6P.	HS	$\sigma\iota$	12.24	3061	40.81	2.0	1.8		L82
0925	SBc(s)II-III	.SXS7..	HS	ι	9.93	792	10.56	13.	8.	115	N73
1087	Sc(s)III.3	.SXT5..	dB	$\sigma\iota$	11.13	1628	21.71	4.	3.	0	N73
1140	Sb pec:	.IB.9P*	dB	$\sigma\iota$	12.11	1560	20.80	1.7	0.9	6	RC3
1255	Sc(s)II	.SXT4..	HS?	–	11.18	1656	22.08	4.6	2.8	117	L82
1300	SBb(s)I.2	.SBT4..	AN	ϵ	10.43	1526	20.35	9.0	7.0	106	L82
1326	RSBa	RLBR+..	–	$\epsilon\sigma$	11.34	1277	19.81	4.8	3.2	77	L82
1365	SBb(s)I	.SBS3..	HS	σ	9.45	1562	19.81	14.0	10.0	32	L82
1415	Sa/SBa late	RSXS0..	HS	$\epsilon\sigma$	11.80	1526	20.35	5.0	2.5	148	L82
1530		.SBT3	HS	κ	11.41	2613	34.84	5.2	2.8	17	N73
2146	SbIIpec	.SBS2P.			10.36	1106	14.75	5.9	4.9	123	N73
2196	Sab(s)I	PSAS1..	AN?	ϵ	11.25	2184	29.12	3.6	3.0	35	L82
2782	Sa(s) pec	.SXT1P.		–	11.50	2574	34.32	4.2	3.2		N73
2903	Sc(s)I-II	.SXT4..	HS	σ	8.91	472	6.29	13.3	6.0	17	N73
2935	SBb(s)I.2	PSXS3..	AN?	ϵ	11.25	2003	26.71	7.0	5.0	0	L82
2997	Sc(s)I.3	.SXT5..	HS	σ	9.62	799	10.65	14.0	13.0		L82
3177	Sb(s)II	.SAT3..	HS	σ	12.45	1220	16.27	1.6	1.3	135	N73
3206		.SBS6..	–	ι	12.31	1224	16.32	3.0	2.0	0	N73
3310	Sbc(r) pec	.SXR4P.	HS	σ	10.84	1073	14.31	3.8	3.5		N73
3346	SBc(rs) II.2	.SBT6..	HS	ι	11.86	1138	15.17	2.6	2.5		N73
3351	SBb(r)II	.SBR3..	HS	σ	9.88	641	8.55	8.5	5.0	13	N73
3359	SBc(s)I.8 pec	.SBT5..	HS	–	10.49	1138	15.17	8.0	4.8	170	N73
3504	Sb(s)/SBb(s)I-II	RSXS2..	–	κ	11.25	1480	19.73	2.5	2.5		N73
3627	Sb(s)II.2	.SXS3..	HS?	ϵ	8.89	593	7.91	9.0	4.2	173	N73
4051	Sbc(s)II	.SXT4..	HS	–	10.56	746	9.95	6.0	5.0	135	N73
4064	SBc(s):	.SBS1*P	HS	ι	11.70	937	15.29	4.2	1.8	150	N73
4124	$SO_3(6)$	.LAR+..	AN?	ϵ	12.35	1501	13.68	4.1	1.8	114	N73
4178	SBc(s)II	.SBT8..	HS	–	11.26	224	13.68	5.5	1.7	30	N73
4212	Sc(s)II-III	.SA.5*.	AN	κ	11.44	-165	13.68	2.9	1.9	75	N73
4245	SBa(s)	.SBRO*.	HS	ϵ	12.25	855	11.40	3.5	3.3		N73
4258	Sb(s)II	.SXS4..	HS	$\epsilon\sigma$	8.04	520	6.93	22.	9.	150	N73
4303	Sc(s)I.2	.SXT4..	AN	–	9.86	1404	15.29	6.6	6.4		N73
4314	SBa(rs) pec	.SBT1..	HS	–	11.35	850	11.33	4.6	4.5		N73
4394	SBb(sr)I-II	RSBR3..	–	–	11.28	853	13.68	3.6	3.4		N73
4457	RSb(rs)II	RSXS0..	–	–	11.12	709	15.29	3.4	2.8		N73
5236	SBc(s)II	.SXS5..	AN	σ	8.08	275	3.40	18.0	18.0		L82
5248	Sbc(s)I-II	.SXT4..	HS	$\epsilon\sigma$	10.42	1049	13.99	6.8	5.0	110	N73
5253	Amorphous	.I..9P*			10.98	147	3.40	6.0	2.0	45	L82
5383	SBb(s)I-II	PSBT3*P	HS	–	11.54	2322	30.96	3.5	2.4	85	N73
5430	SBb(r)II	.SBS3..	–	–	12.10	3016	40.21	2.3	1.6	0	N73
5597	SBc(s)II	.SXS6..	HS	$\epsilon\sigma$	12.20	2444	32.59	2.1	1.7	60	RC3
6217	RSBbc(s)II	RSBT4..	–		11.41	1598	21.31	3.6	3.6		N73
6951	Sb/SBb(rs)I.3	.SXT4..	HS	ϵ	11.31	1710	22.80	4.0	3.6	170	N73
7741	SBc(s)II.2	.SBS6..	HS	ι	11.37	1030	13.73	4.4	2.9	170	N73

arranged as follows – column 1: the name of the galaxy; columns 2 and 3: the structure of the galaxy from the Revised Shapley–Ames (RSA) catalogue (Sandage & Tammann 1981), and the Third Reference Catalogue of Bright Galaxies (de Vaucouleurs et al. 1991), hereinafter referred to as RC3; columns 4 and 5: morphological type of the nucleus as classified by Sérsic (1973) and Prabhu (1980). Sérsic (1973) classified the nuclear regions into those with either amorphous nuclei (AN) or hotspot (HS) systems, while Prabhu (1980) developed a somewhat more elaborate scheme. In this scheme, the galaxies are classified on the relative prominence of the unresolved or barely resolved nuclear region, which in their seeing-limited photographs was taken to be less than 4 arcsec, and the circumnuclear structure, which can extend from about 10 to 30 arcsec from the nuclear region. The different classes are as follows:

class κ has a very bright nucleus with circumnuclear formation which is very faint or absent;

class ε has a bright nucleus and a bright circumnuclear formation which is elliptical and has a smooth intensity distribution;

class σ has a bright nucleus and distinct hotspots or spiral pattern in the circumnuclear region;

class ι has at best a very faint nucleus with a bar-like formation of faint hotspots.

In the intermediate class $\varepsilon\sigma$, the circumnuclear formation does not have a well-defined boundary, while in the $\sigma\iota$ class the circumnuclear formation is bar-like, generally resolved into hotspots.

Columns 6 and 7 of Table 1 give the blue magnitude $B_T^{0,i}$ and the recession velocity taken from the RSA catalogue, except for NGC 1530 and 3206, whose values are from RC3. Column 8 gives the distance in Mpc, estimated using a Hubble constant of $H_0 = 75$ km s^{-1} Mpc^{-1}. For sources which are in the groups listed in the RSA catalogue, the mean velocity of the group has been used for calculating the distance. Columns 9 to 12 give the major and minor axes in arcmin and the position angle (PA) of the optical galaxy in deg, and the reference for this information, which is coded as follows – L82: Lauberts (1982); N73: Nilson (1973); and RC3: The Third Reference Catalogue of Bright Galaxies.

3 OBSERVATIONS AND OBSERVATIONAL RESULTS

The observations were made with the VLA A-array at 20 cm on 1983 September 11 and with the B-array at 6 cm on 1988 February 1. This is true for all the sources except NGC 3310, which was observed on 1986 August 16. The data were calibrated in the standard way, using the DEC10 at the VLA, with 3C 286 as the primary flux density calibrator. The flux densities are on the BGPW scale (Baars et al. 1977).

The radio images of the galaxies are presented in Fig. 1, while the observational parameters and observed properties are summarized in Table 2, which is arranged as follows – column 1: name of the galaxy; column 2: wavelength of the observations in cm; column 3: major and minor axes of the restoring beam in arcsec and its PA in deg; column 4: the rms noise in the image in units of mJy beam^{-1}; column 5: name of the component, where O refers to the optical galaxy; columns 6 and 7: Right Ascension and Declination in B1950 coordinates of the pixel of maximum brightness of the radio component except when it is preceded by the letter 'O', in which case it refers to the position of the optical galaxy; and columns 8 and 9: the peak brightness in units of mJy beam^{-1} and the total flux density in mJy for the corresponding component. In the row marked 'O', the peak and total flux densities refer to the entire image shown in the figures, except in the case of NGC 5248 where we show the image of a possibly unrelated source in the field. The positions of the optical galaxies have been taken from the NED compilation (Helou et al. 1991).

4 NOTES ON INDIVIDUAL SOURCES

NGC 210. The peak brightness at 20 cm with a restoring beam of 0.8 arcmin is 3.6 mJy beam^{-1} (Condon 1987).

NGC 255. Hummel et al. (1985) detected extended emission with a total flux density of 21 ± 5 mJy at 20 cm with an angular resolution of 15 arcsec.

NGC 613. A low-resolution VLA C/D-array image at 20 cm with an angular resolution of 60 arcsec shows the total flux density to be 220 mJy (Condon 1987). Hummel & Jörsäter (1992) present high-resolution images which resolve the central component into a linear feature with three discrete components, the central one of which is likely to be the nucleus. The W and E components in our image are resolved into a ring-like feature.

NGC 922. The peak brightnesses in the 20 cm image with an angular resolution of 21 arcsec are 11.4 and 7.6 mJy beam^{-1}, respectively, while the total flux density is 59.3 mJy (Condon et al. 1990). The components we detected are close to the total intensity peaks in the low-resolution image.

NGC 925. Images at 20 cm with resolutions of 48 arcsec and about 40 arcsec have been presented by Condon (1987) and Gioia & Fabbiano (1987), respectively. The compact feature, which has a flux density of 0.8 mJy, is north of the centre of the galaxy and the peak of radio emission in the low-resolution images by about 40 arcsec.

NGC 1087. VLA D-array images at 20 cm show the source to be resolved along a PA $\sim 81°$ with a total flux density of 133 mJy (Condon 1987; Condon et al. 1990). The peaks of emission seen in our images are offset from the nucleus, and have non-thermal spectra with spectral indices of about 0.5, 0.7, 0.7 and 0.8 for E1, E2, E3 and E4, respectively.

NGC 1140. Comparison of the 20- and 6-cm images shows that the spectral index of the emission within the contour box is ~ 0.5, while that of the dominant component is significantly flatter with $\alpha \sim 0.2$. A 20-cm image has also been published by Neff & Hutchings (1992).

NGC 1255. Images at 20 cm with resolutions of 60 and 28 arcsec have been published by Condon (1987) and Hummel et al. (1985), respectively. The total flux density at this wavelength is 32.5 mJy (Condon 1987).

NGC 1300. VLA C-array and D-array images show radio emission which is related to the optical bar and the chain of H II regions at the end of it (Hummel et al. 1985; Condon 1987). The location of the three main components in our 20- and 6-cm images suggests that there might be collimated outflow of material from an active nucleus. The spectral

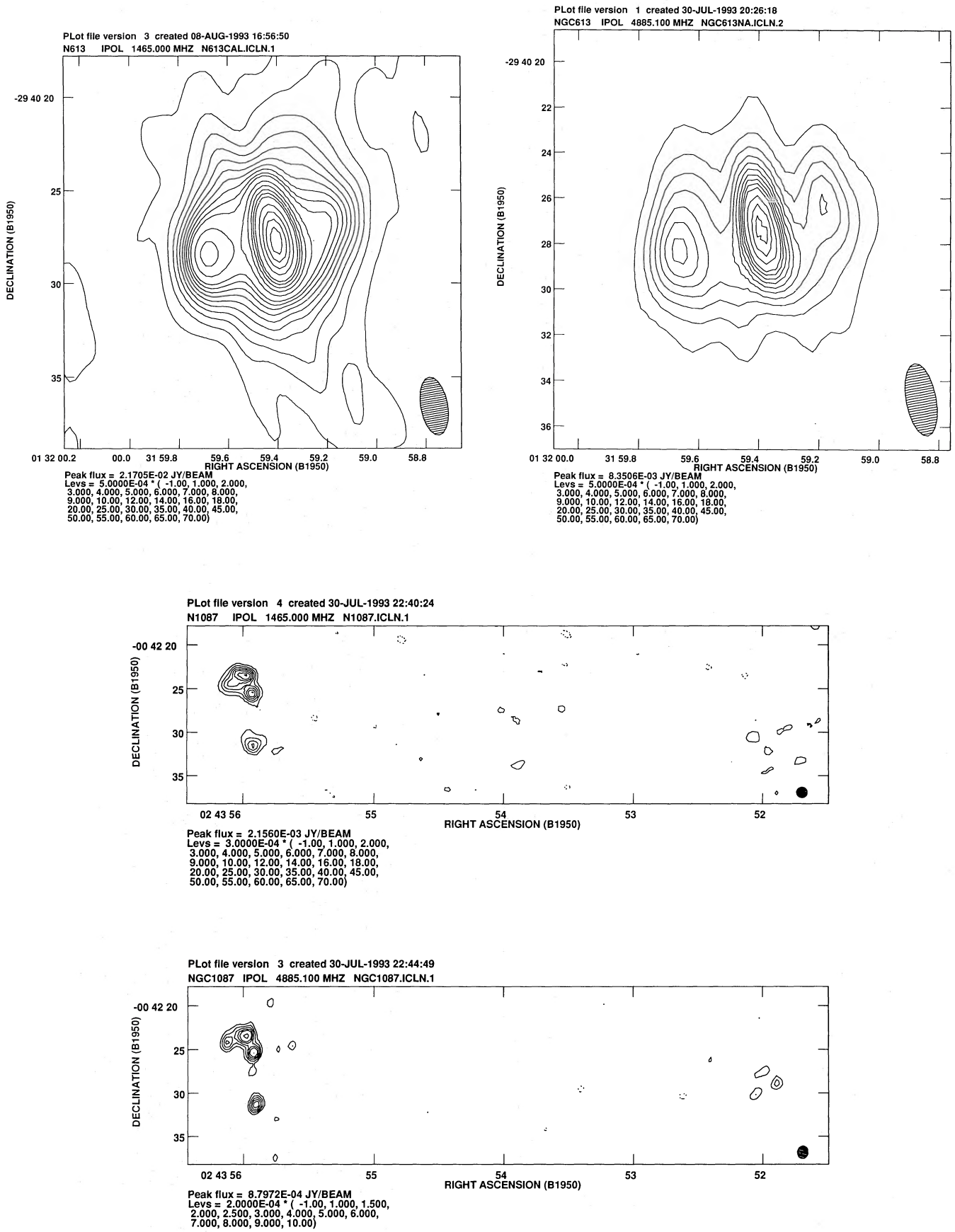

Figure 1. Radio images of the sample of Sérsic–Pastoriza galaxies.

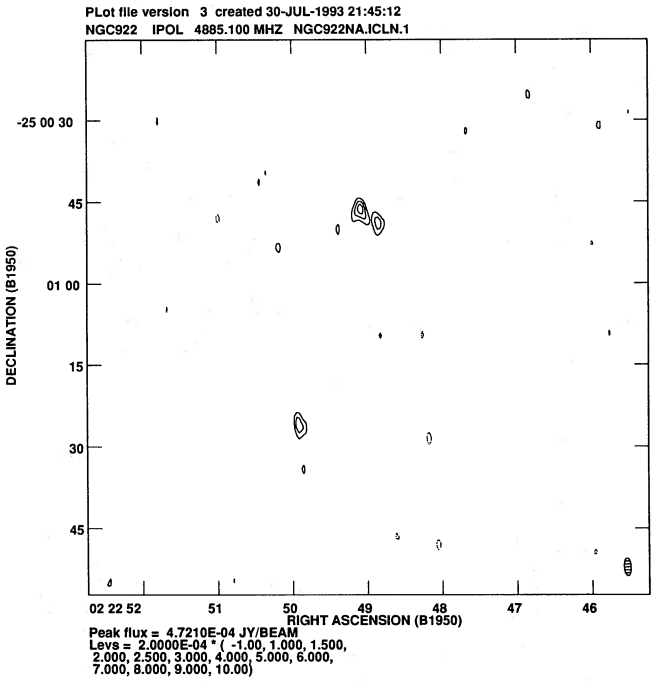

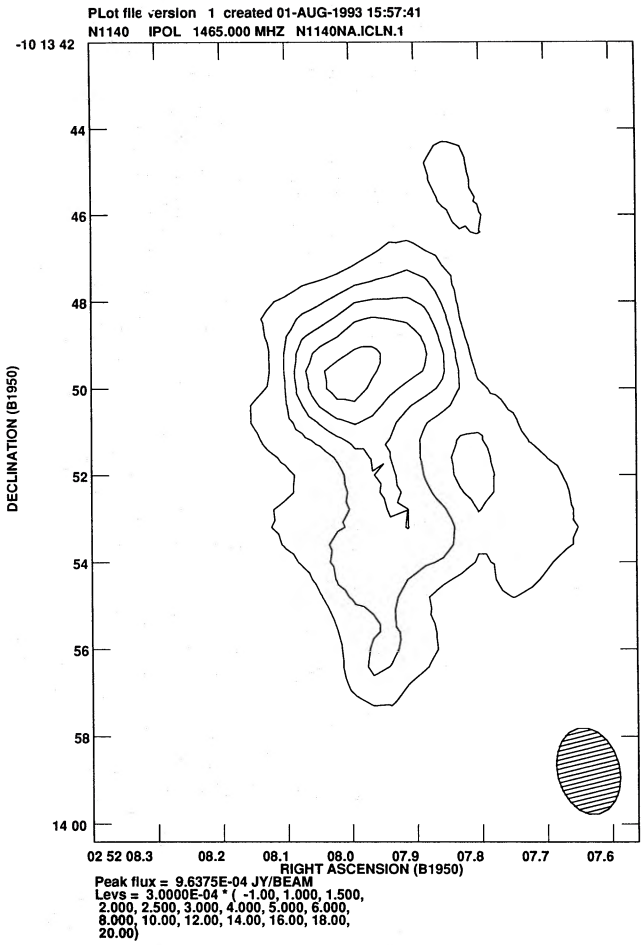

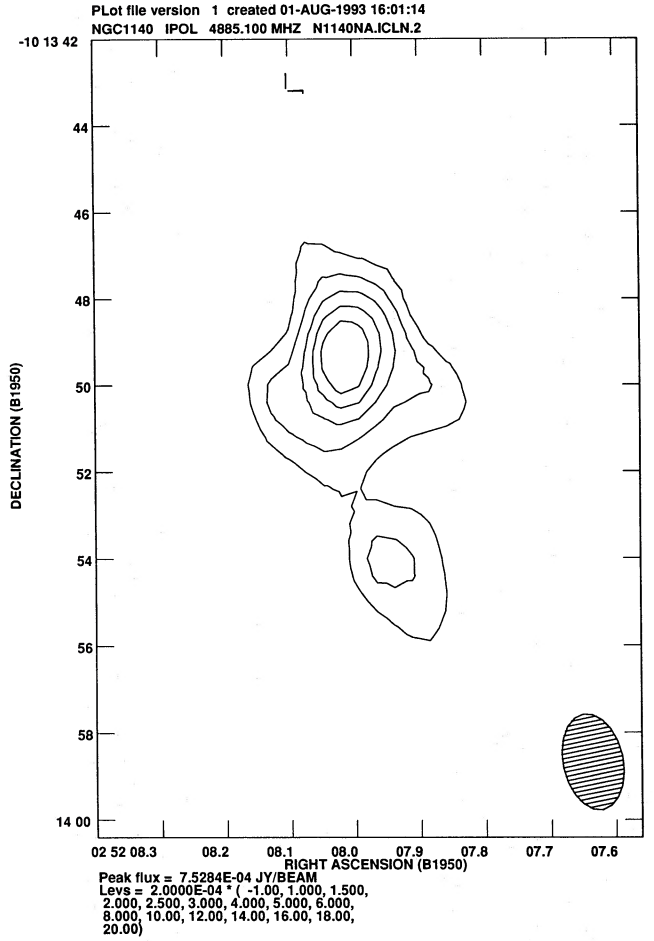

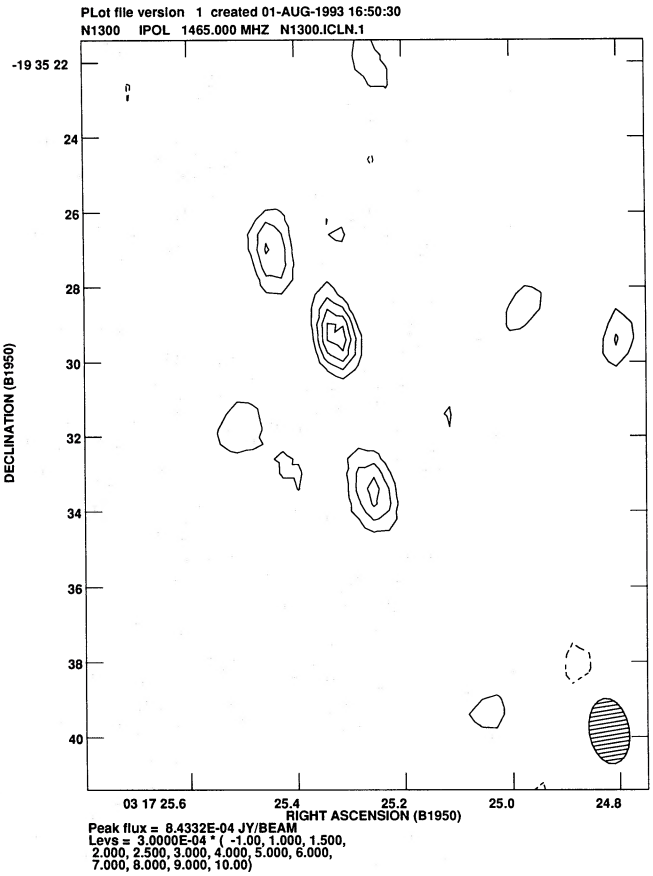

Figure 1 – *continued*

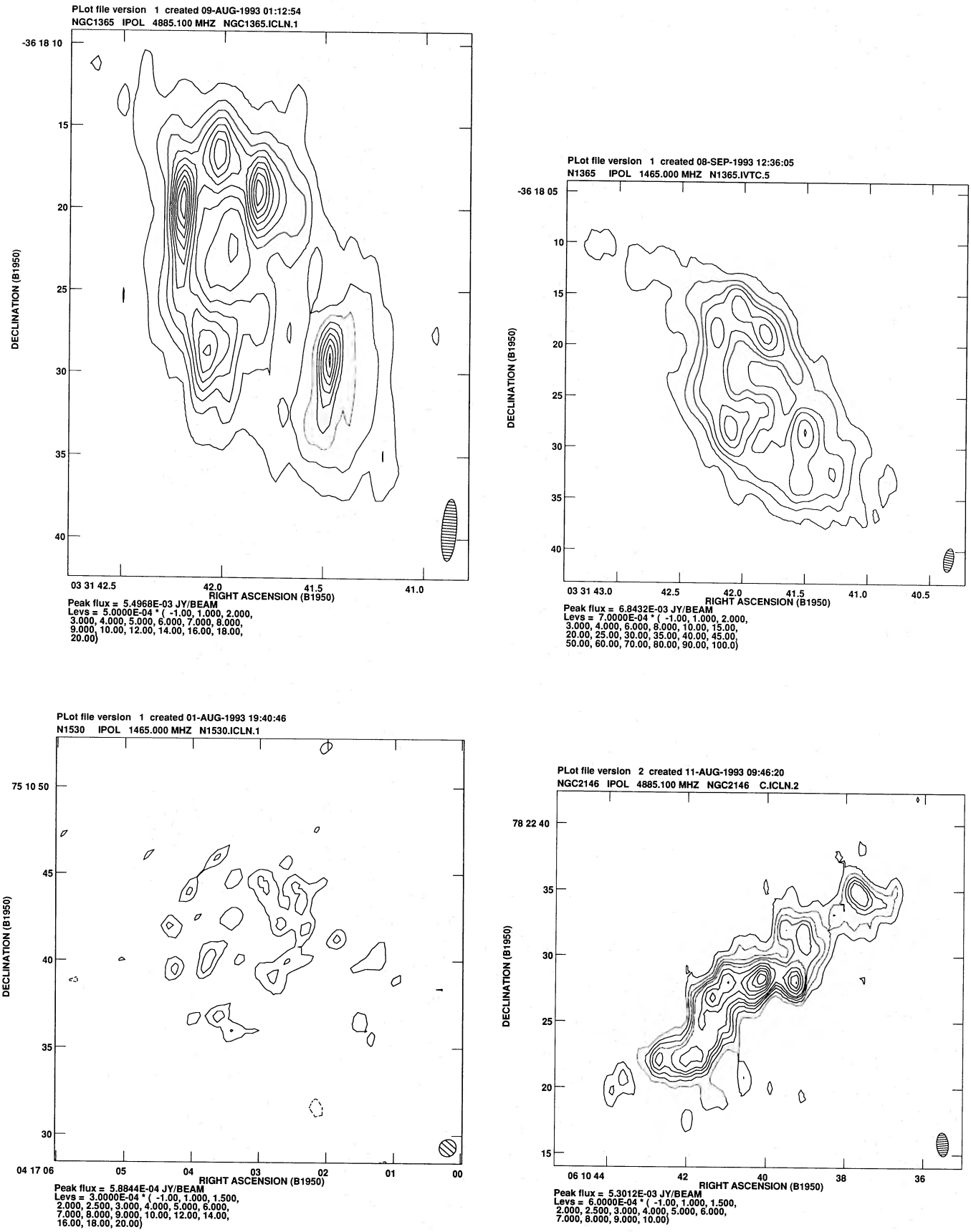

Figure 1 – *continued*

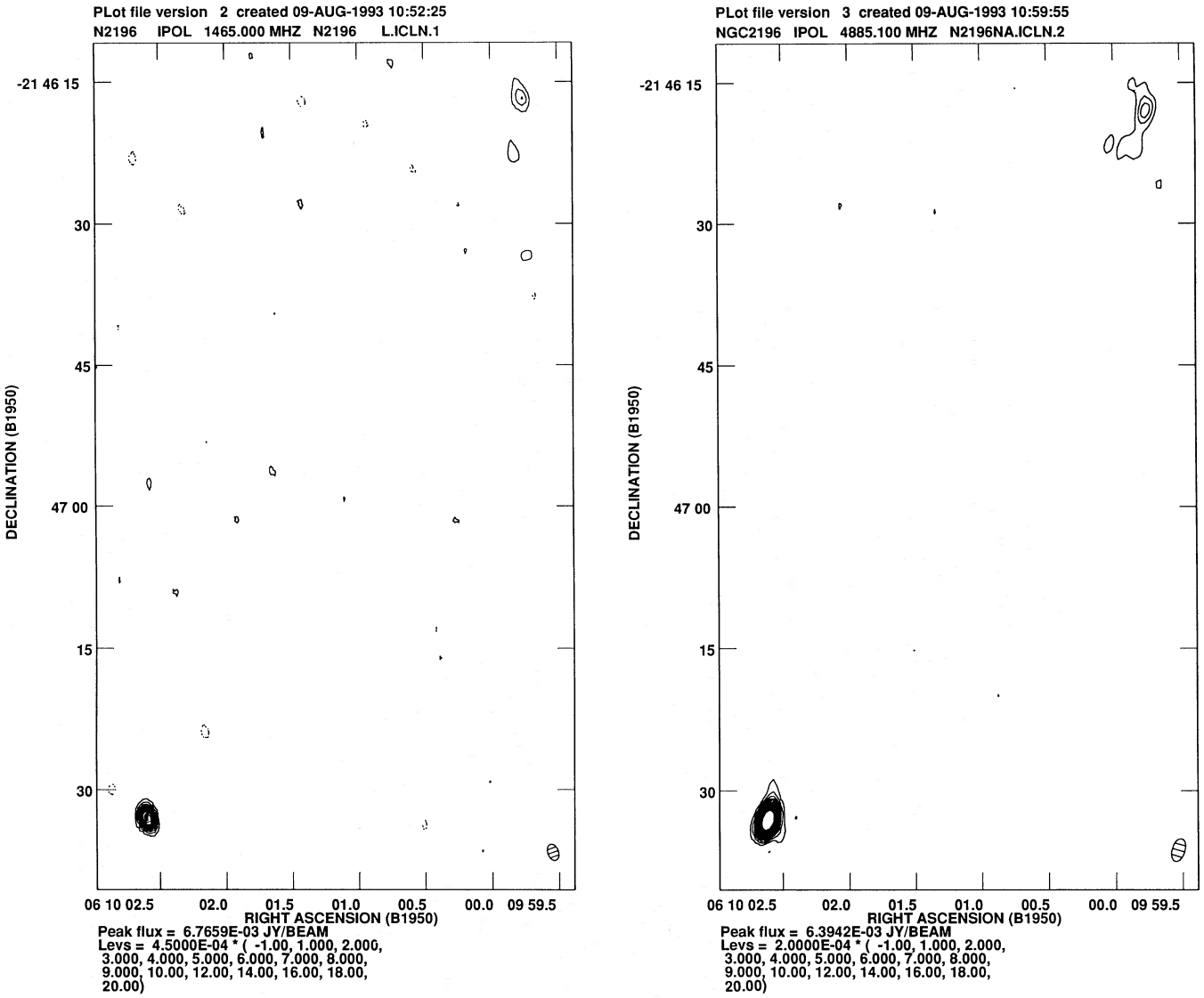

Figure 1 – *continued*

index of the dominant component, which is the only one we detect at 6 cm, is rather flat with $\alpha \sim 0.2$.

NGC 1326. Condon (1987) detected an unresolved component with an angular resolution of 60 arcsec at 20 cm; the total flux density of the component is about 30 mJy.

NGC 1365. A 20-cm VLA image with a resolution of 48 arcsec (Condon 1987) and a MOST image at 843 MHz with a resolution of about 40×70 arcsec^2 (Harnett 1987) reveal the large-scale structure of the source, while the higher resolution observations with the partial-VLA at 20 and 6 cm by Sandqvist, Jörsäter & Lindblad (1982) show the ring of emission in the central region. Our 20-cm image shows the structure of the ring in greater detail and also shows evidence of radio emission near the nucleus of the galaxy. The spectral index of the entire emission is about 0.9 between 20 and 6 cm. This galaxy is being studied at radio and optical wavelengths by Sandqvist et al. (1994, in preparation).

NGC 1415. VLA 20-cm observations with resolutions of 21 and 8 arcsec yield peak flux densities of 14.7 and 6.1 mJy beam^{-1}, respectively (Condon et al. 1990).

NGC 2146. Low-resolution observations have been made with the VLA at 20 cm (Condon 1983), WSRT at 20 and 6 cm (de Bruyn 1977), and at higher resolutions with the VLA and the NRAO interferometer (Kronberg & Biermann 1981; Condon et al. 1982; Carral, Turner & Ho 1990).

NGC 2782. Low-resolution VLA images at 20 cm show the source to be extended along a PA $\sim 160°$ with a total flux density of 110 mJy. The A-array 20-cm image (Condon et al. 1982) and the one made with the incomplete VLA by Wilson & Willis (1980) show features that are similar to our image. The compact component was not detected at 15 GHz with a resolution of 0.18×0.15 arcsec^2 to a limit of 0.3 mJy beam^{-1} (Carral et al. 1990).

NGC 2903. Images at 20 cm with the VLA D- and C-arrays and with the WSRT (Condon 1987; Hummel et al. 1985; van der Kruit 1973) show the emission from the disc of the galaxy. Higher resolution observations of the central region have been published by van der Hulst, Crane & Keel (1981), Wynn-Williams & Becklin (1985) and Vila et al. (1990). Our images are of marginally higher resolution than

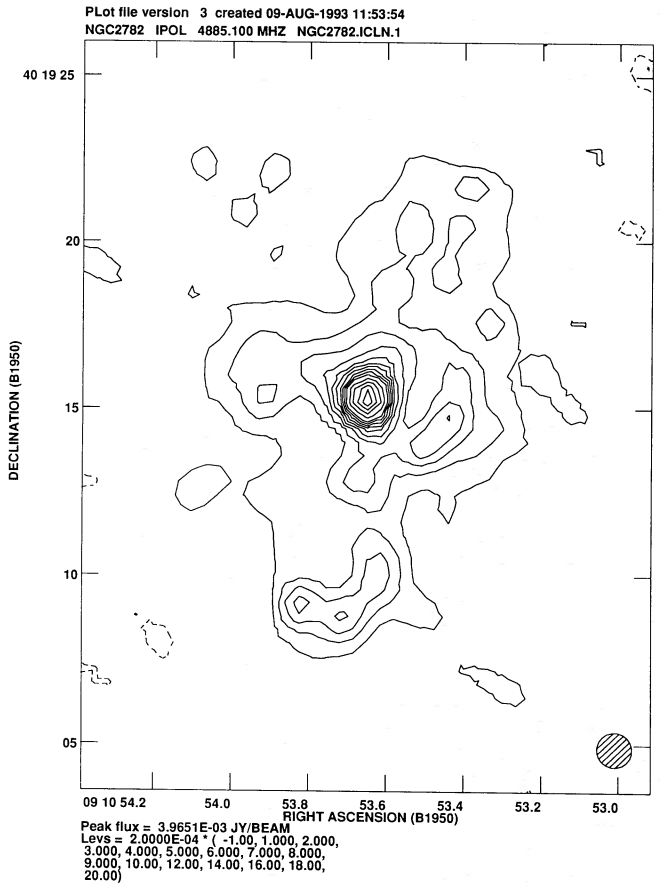

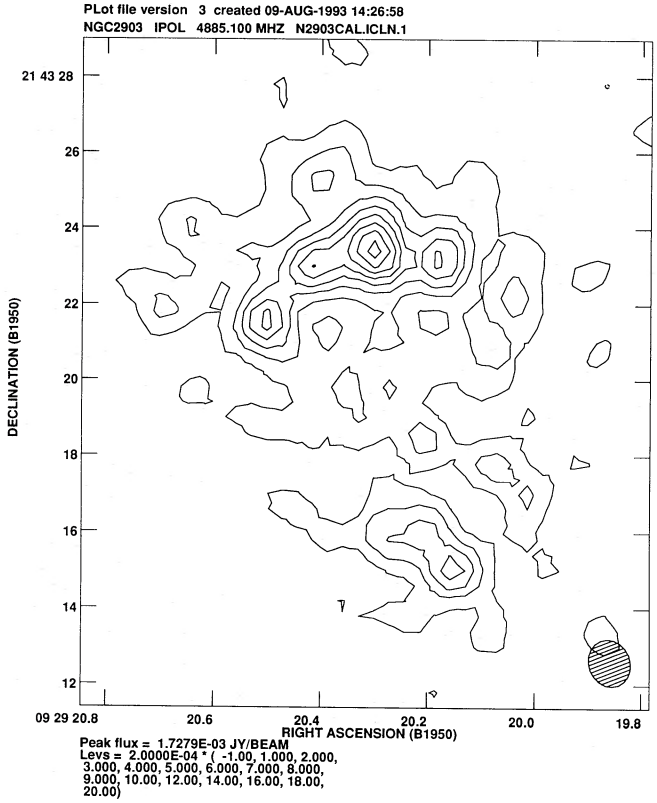

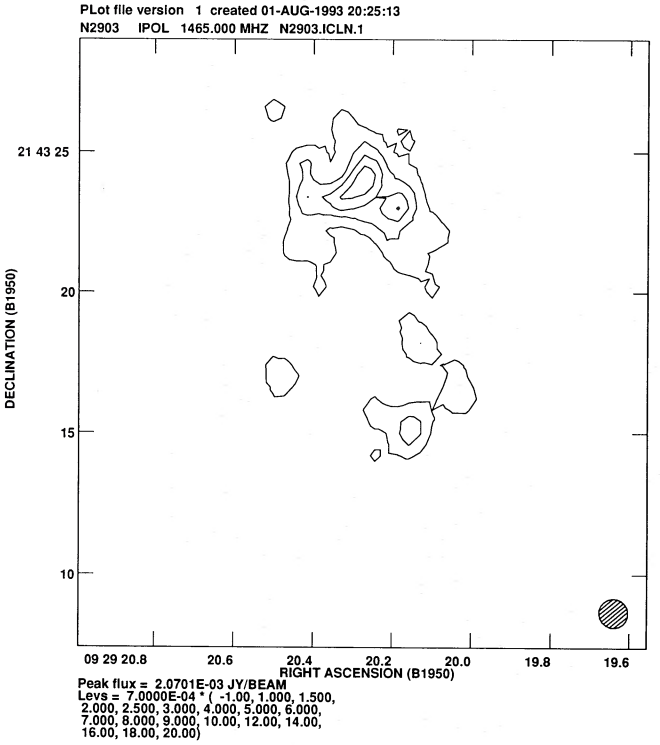

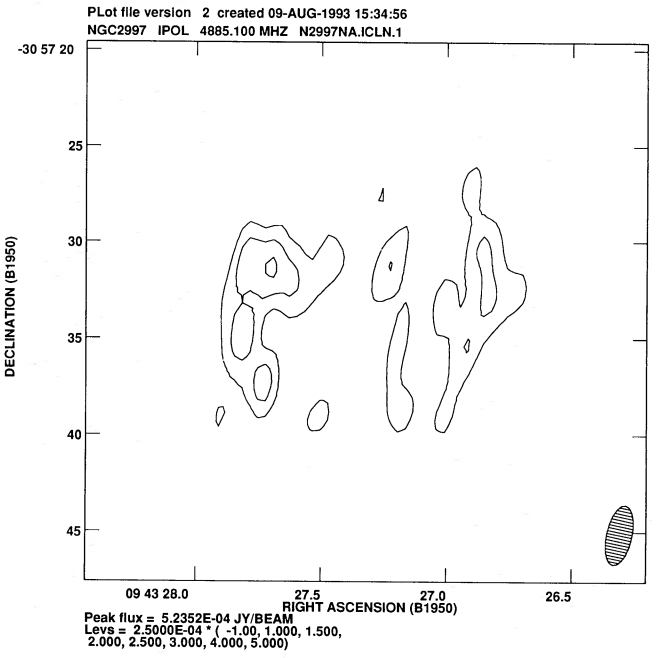

Figure 1 – *continued*

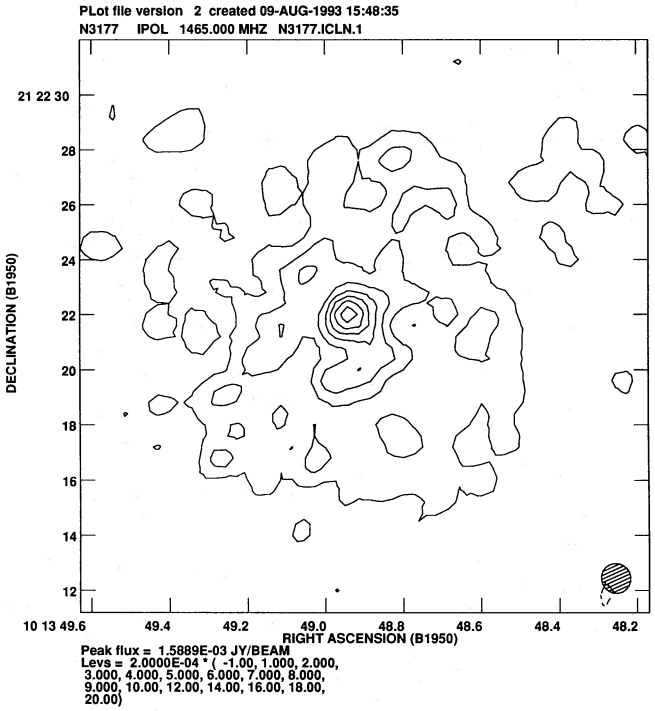

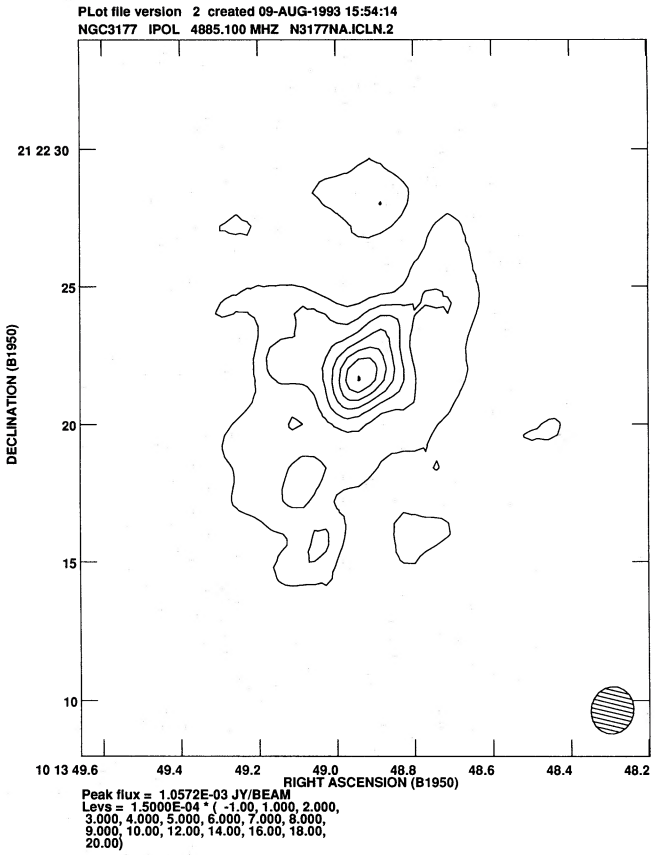

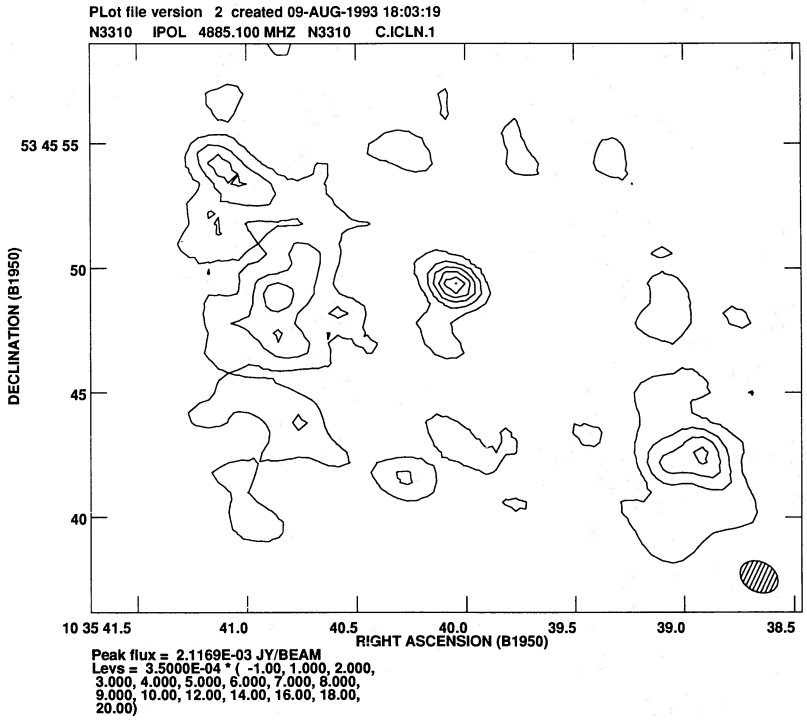

Figure 1 – *continued*

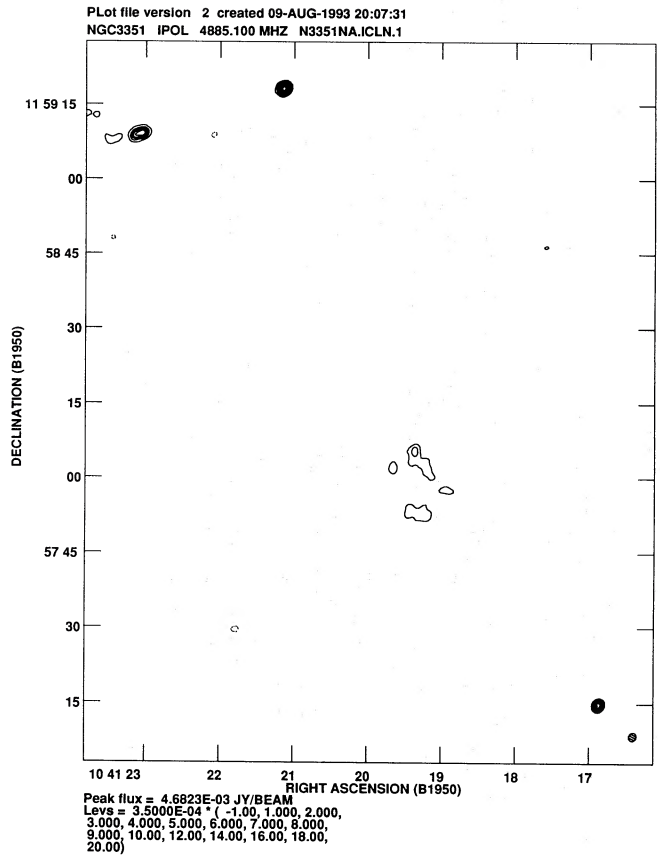

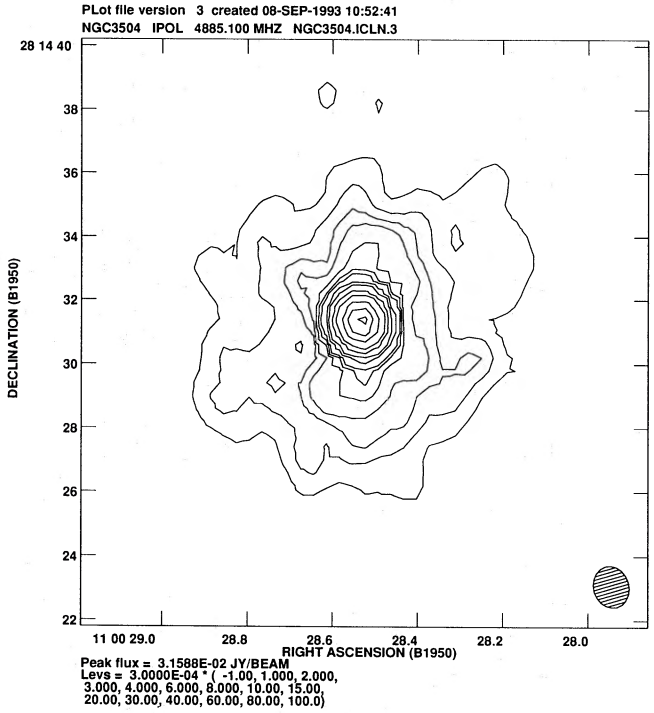

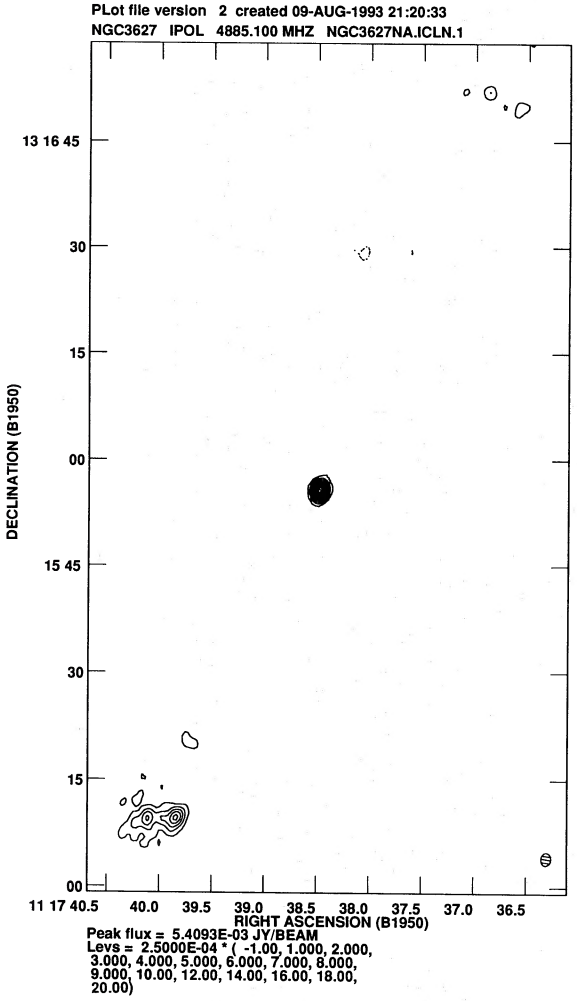

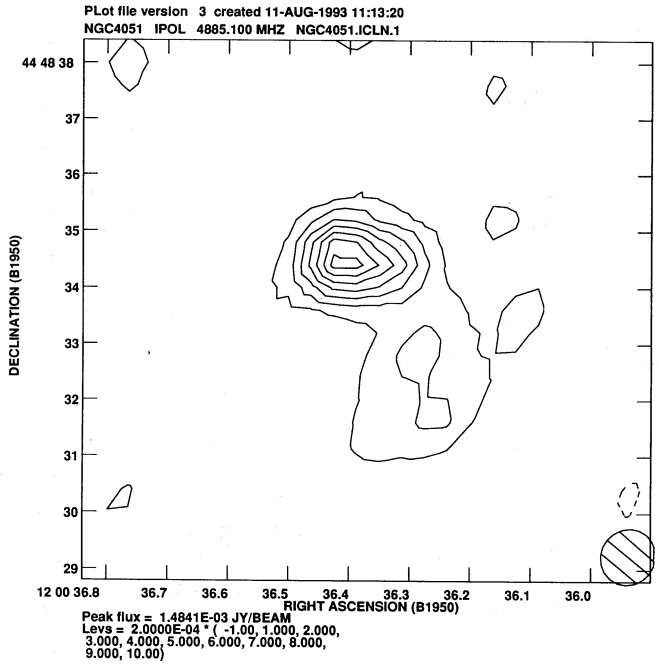

Figure 1 – *continued*

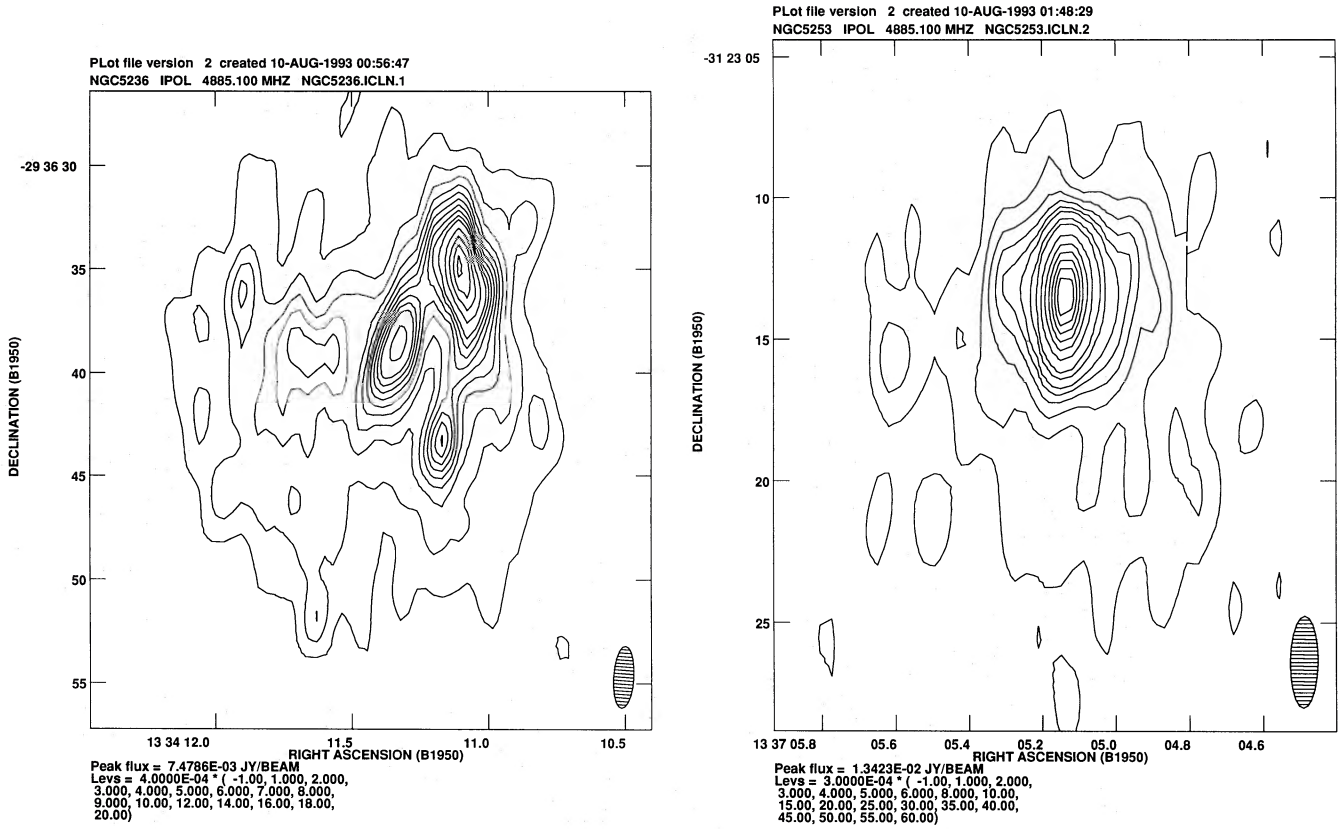

Figure 1 – *continued*

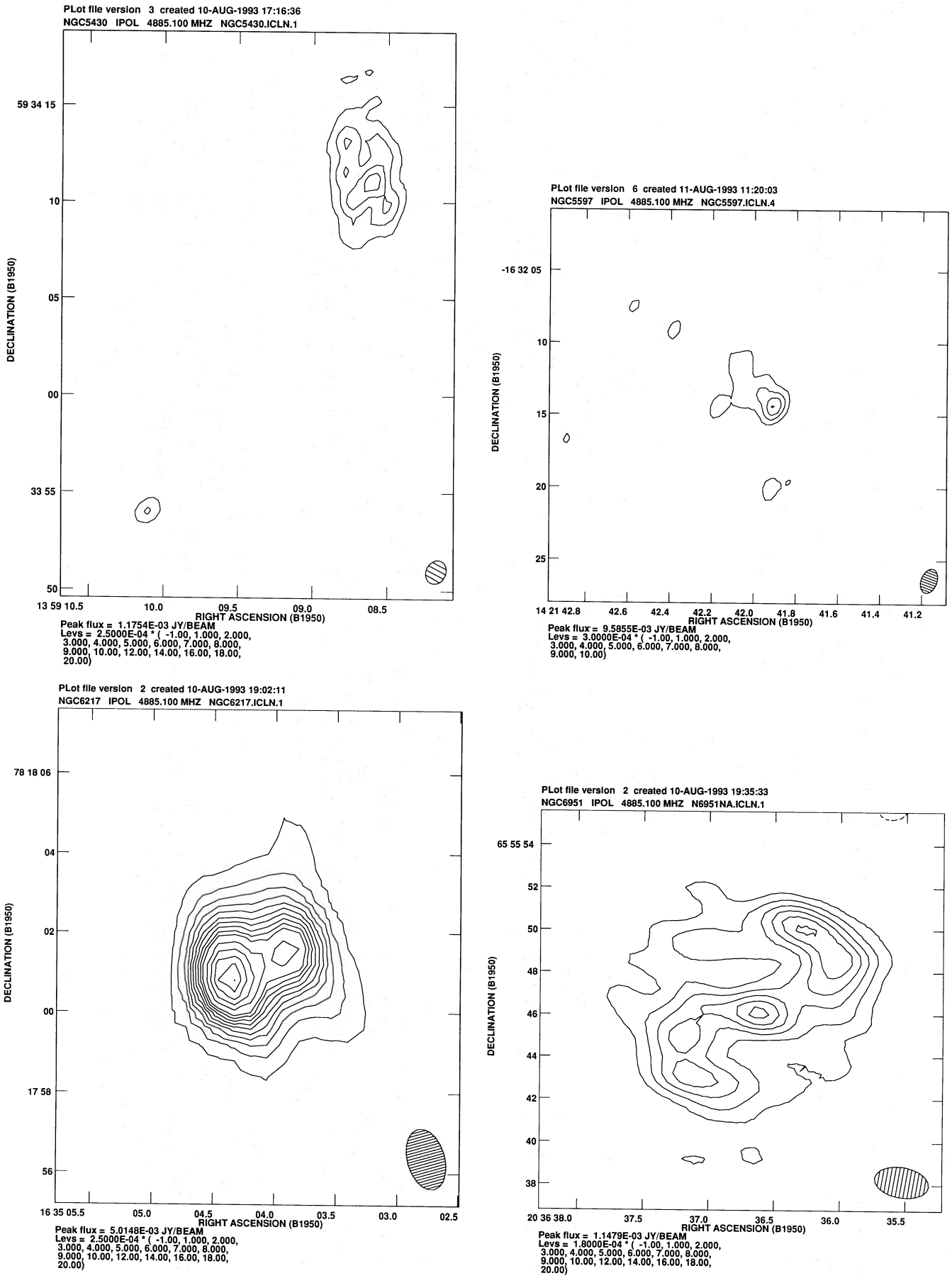

Figure 1 – *continued*

Table 2. Observational parameters and observed properties of individual sources.

Galaxy	Observational parameters					Cmp.	Observed properties							
		Beam size			σ_t		Radio position (B1950)						Flux density	
	λ	maj.	min.	PA			R.A.			Dec.			peak	total
NGC	cm	"	"	°	mJy/b		h	m	s	°	′	"	mJy/b	mJy
(1)	(2)		(3)		(4)	(5)		(6)			(7)		(8)	(9)
0210	20	1.67	1.18	8	0.14	O	00	38	03.9	-14	08	48	≤0.5	
0255	20	1.56	1.19	8	0.14	O	00	45	16.2	-11	44	27	≤0.5	
0613	20	3.12	1.45	10	0.08	W	01	31	59.25	-29	40	27.4	5.8	
						C			59.41			27.7	21.7	
						E			59.69			28.6	7.5	
						O			59.00			30.0	21.7	115
	6	3.21	1.32	11	0.07	W	01	31	59.18	-29	40	26.2	2.6	
						C			59.41			27.4	8.4	
						E			59.65			28.2	3.7	
						O			59.00			30.0	8.4	42
0922	6	3.30	1.29	4	0.06	N1	02	22	48.85	-25	00	48.8	0.4	0.7
						N2			49.09			46.4	0.5	1.2
						S			49.91		01	26.0	0.4	0.9
						O	02	22	48.00	-25	00	54.0		
0925	6	1.78	1.63	114	0.05	A	02	24	15.32	33	22	01.6	0.8	0.8
						O			16.60		21	20.0		
1087	20	1.24	1.24		0.11	E1	02	43	55.92	-00	42	31.4	1.3	
						E2			55.92			25.4	1.8	
						E3			55.97			23.4	2.2	
						E4			56.11			24.6	1.3	
						O			51.60			19.0	2.2	19
	6	1.50	1.23	168	0.06	E1	02	43	55.89	-00	42	31.4	0.7	
						E2			55.92			25.4	0.8	
						E3			55.97			23.4	0.9	
						E4			56.13			24.2	0.5	
						O			51.60			19.0	0.9	9
1140	20	2.02	1.43	14	0.10	C	02	52	08.00	-10	13	49.6	1.0	
						O			08.02			49.0	1.0	11
	6	2.24	1.38	11	0.04	C	02	52	08.02	-10	13	49.2	0.8	
						O			08.02			49.0	0.8	6
1255	6	2.66	0.98	4	0.08	O	03	11	22.00	-25	54	36.0	≤0.5	
1300	20	1.76	1.08	9	0.12	S	03	17	25.26	-19	35	33.4	0.7	
						C			25.31			29.4	0.8	
						N			25.45			27.0	0.6	
						O			25.30			39.0	0.8	7
	6	2.21	1.01	180	0.07	C	03	17	25.31	-19	35	29.4	0.6	0.6
1326	20	2.32	1.02	15	0.25	O	03	22	01.00	-36	38	24.0	≤1	
1365	20	2.32	0.95	170	0.26	A1	03	31	41.50	-36	18	28.4	5.7	
						A2			41.83			18.8	6.6	
						A3			42.03			16.4	5.5	
						A4			42.20			18.8	5.1	
						A5			42.10			28.0	6.8	
						O			41.00			24.0	8.2	338
	6	3.81	0.90	176	0.14	B1	03	31	41.47	-36	18	29.2	4.6	
						B2			41.83			19.2	4.9	
						B3			42.03			16.8	4.0	
						B4			42.20			19.6	5.5	
						B5			42.07			28.8	3.5	
						O			41.00			24.0	5.5	127
1415	20	1.50	1.04	26	0.20	O	03	38	46.00	-22	43	24.0	≤0.9	
1530	20	1.02	0.97	139	0.11	O	04	17	04.90	75	10	48.0	0.6	28
2146	6	1.81	0.90	5	0.19	A1	06	10	37.65	78	22	34.8	2.4	
						A2			39.11			31.6	2.3	
						A3			39.24			28.0	4.3	
						A4			40.17			28.4	5.3	
						A5			40.96			28.0	3.6	
						A6			41.36			26.8	3.9	
						A7			41.76			22.4	2.7	
						A8			42.02			22.0	2.7	
						A9			42.68			22.0	2.0	
						O			40.10			23.0	5.3	160
2196	20	1.78	1.13	20	0.15	W	06	09	59.76	-21	46	16.8	1.4	7
						E		10	02.60		47	32.8	6.8	8
						O		10	03.00		47	36.0	6.8	26
	6	2.47	1.35	164	0.05	W	06	09	59.76	-21	46	18.0	0.8	3
						E		10	02.60		47	33.2	6.4	7
						O		10	03.00		47	36.0	6.4	9
2782	6	1.05	1.04	44	0.09	W	09	10	53.44	40	19	14.8	1	
						C			53.65			15.2	4.0	

Table 2 – *continued*

Galaxy	Observational parameters					Cmp.	Observed properties							
		Beam size			σ_t		Radio position (B1950)						Flux density	
	λ	maj.	min.	PA			R.A.			Dec.			peak	total
NGC	cm	"	"	°	mJy/b		h	m	s	°	′	"	mJy/b	mJy
(1)	(2)		(3)		(4)	(5)		(6)			(7)		(8)	(9)
						E			53.90			15.6	0.6	
						S1			53.62			10.0	0.7	
						S2			53.72			08.8	0.9	
						S3			53.83			09.2	0.9	
						O			53.85			17.0	4	40
2903	20	1.05	1.03	40	0.22	N1	09	29	20.19	21	43	23.0	1.8	
						N2			20.27			24.2	2.1	
						O			19.90			19.0	2.1	66
	6	1.26	1.08	22	0.09	N1	09	29	20.19	21	43	23.0	1.0	
						N2			20.30			23.4	1.7	
						N3			20.42			23.0	1.2	
						N4			20.50			21.4	1.1	
						S1			20.16			15.0	0.9	
						O			19.90			19.0	1.7	29
2935	20	1.87	1.08	2	0.17	O	09	34	26.00	-20	54	12.0	$\leq$0.8	
	6	2.24	0.99	174	0.07	O	09	34	26.00	-20	54	12.0	$\leq$0.4	
2997	20	2.58	1.02	4	0.19	O	09	43	28.00	-30	57	36.0	$\leq$ 0.8	
	6	3.17	1.33	168	0.06	O	09	43	28.00	-30	57	36.0	0.5	14
3177	20	1.10	1.06	24	0.09	C	10	13	48.94	21	22	22.0	1.6	
						O			49.20			28.0	1.6	53
	6	1.72	1.55	167	0.05	C	10	13	48.94	21	22	21.6	1.1	
						O			49.20			28.0	1.1	13
3206	6	1.73	1.38	54	0.07	O	10	18	30.40	57	10	58.0	$\leq$0.4	
3310	6	1.63	1.22	64	0.11	W	10	35	38.92	53	45	42.6	1.5	
						C			40.05			49.4	2.1	
						E1			40.86			49.0	1.3	
						E2			41.13			54.2	1.2	
						O			40.30			45.0	2.1	63
3346	6	1.44	1.28	180	0.07	O	10	40	59.00	15	08	03.0	$\leq$0.5	
3351	6	1.75	1.53	153	0.10	S	10	41	16.88	11	57	14.8	2.1	2.2
						CR			19.36		58	05.6	0.9	18
						O			19.60		58	00.0		
						N1			21.14		59	18.0	4.7	5.9
						N2			23.04		59	09.2	2.1	5.8
3359	6	1.91	1.30	57	0.08	O	10	43	21.10	63	29	11.0	$\leq$0.5	
3504	6	1.25	1.04	21	0.10	C	11	00	28.52	28	14	31.4	30	
						O			28.50			31.0	30	68
3627	6	1.79	1.40	171	0.07	C	11	17	38.49	13	15	55.6	5.4	7
						S1			39.83			09.6	1.3	
						S2			40.11			09.6	1.1	
						O			38.70			32.0	5.4	18
4051	6	1.02	0.96	140	0.07	C	12	00	36.39	44	48	34.4	1.5	
						O			36.41			34.8	1.5	9
4064	20	1.10	1.06	33	0.10	O	12	01	37.30	18	43	16.0	$\leq$0.6	
4124	6	1.44	1.20	180	0.07	O	12	05	35.80	10	39	27.0	$\leq$0.4	
4178	6	1.41	1.17	170	0.07	O	12	10	13.10	11	08	30.0	$\leq$0.4	
4212	6	1.42	1.20	2	0.07	O	12	13	06.40	14	10	45.0	$\leq$0.4	
4245	6	1.22	1.17	38	0.07	O	12	15	05.74	29	53	08.4	$\leq$0.4	
4258	6	1.00	0.95	139	0.07	C	12	16	29.38	47	34	53.0	1.5	2
						O			29.79			51.0		
4303	6	1.49	1.15	176	0.09	O	12	19	21.62	04	45	03.3	$\leq$0.6	
4314	6	1.29	1.03	13	0.07	O	12	20	01.80	30	10	21.0	$\leq$0.4	
4394	6	1.36	1.09	2	0.06	O	12	23	24.70	18	29	30.0	$\leq$0.3	
4457	6	1.43	1.17	172	0.06	C	12	26	25.79	03	50	49.2	1.9	2.7
						O			26.00			51.0		
5236	6	2.98	0.98	176	0.13	A1	13	34	11.11	-29	36	34.8	7.5	
						A2			11.17			43.2	3.7	
						A3			11.32			38.4	5.2	
						A4			11.66			39.2	2.3	
						O			11.00			48.0	7.5	145
5248	6	1.33	1.11	160	0.13	O	13	35	02.40	09	08	23.0	$\leq$0.5	
						W[g]	13	34	59.85	09	10	16.6	12.3	16
						C[g]		34	59.94			17.6	1.8	1.8
						E[g]		35	00.22			19.3	6.5	15
						Tot		34	59.84			16.4	11	33
5253	6	3.22	0.98	179	0.10	C	13	37	05.15	-31	23	13.6	13.4	
						O			05.00			30.0	13.4	55
5383	6	1.26	1.05	155	0.08	O	13	55	00.35	42	05	22.8	$\leq$0.5	
5430	6	1.24	1.02	152	0.08	W1	13	59	08.53	59	34	09.6	0.8	
						W2			08.58			11.2	1.2	

Table 2 – *continued*

Galaxy	Observational parameters					Cmp.	Observed properties							
		Beam size			σ_t		Radio position (B1950)						Flux density	
	λ	maj.	min.	PA			R.A.			Dec.			peak	total
NGC	cm	"	"	°	mJy/b		h	m	s	°	′	″	mJy/b	mJy
(1)	(2)		(3)		(4)	(5)		(6)			(7)		(8)	(9)
						W3			08.74			10.0	1.0	
						W4			08.79			11.6	0.8	
						W5			08.79			13.2	0.8	
						WR			08.58			11.2	1.2	11
						O			08.50			16.0		
						E			10.11		33	54.0	0.6	0.7
5597	6	1.75	1.11	159	0.13	C	14	21	41.92	-16	32	14.4	1.2	
						G			42.00			14.0	1.2	12
						S[g]			38.74		35	49.8	10.9	13
6217	6	1.56	0.94	16	0.08	W[g]	16	35	03.85	78	18	01.6	3.0	5.4
						E[g]			04.36			00.9	4.8	10
						O			05.10			05.0	5.0	21
6951	6	2.57	1.44	80	0.06	W1	20	36	36.07	65	55	48.8	1.1	
						W2			36.26			50.0	1.1	
						C			36.59			46.0	1.1	
						E1			37.18			44.8	0.8	
						E2			37.11			43.2	0.9	
						O			37.70			48.0	1.1	14
7741	20	1.15	1.09	175	0.25	O	23	41	22.70	25	47	53.0	≤1	

those reported earlier, and appear to resolve the northern feature into a number of components.

NGC 2935. Condon (1987) presented a VLA 20-cm image with 48-arcsec resolution and listed two components which are separated by 6 arcsec and have peak brightnesses of 8.6 and 6.8 mJy beam^{-1}, the total flux density being about 40 mJy.

NGC 2997. VLA 20-cm image with 48-arcsec resolution shows extended emission with a peak brightness of 41.3 mJy beam^{-1} and a total flux density of 290 mJy (Condon 1987).

NGC 3177. Condon et al. (1990) presented VLA 20-cm images with angular resolutions of 15 and 5 arcsec, where the peak brightnesses are 24.6 and 8 mJy beam^{-1}, respectively, while the total flux density estimated from the lower resolution image is 41.8 mJy.

NGC 3310. Low-resolution observations at 20 cm with 60-arcsec resolution show a single component which has peak and total flux densities of 254 mJy beam^{-1} and 383 mJy, respectively (Condon 1987). The VLA C-array 20-cm image (Condon 1983; Hummel et al. 1985) and 6-cm WSRT observations (van der Kruit & de Bruyn 1976) show more detailed structure in the emission, while higher resolution observations show several compact knots of radio emission (Balick & Heckman 1981; Duric et al. 1986; Vila et al. 1990).

NGC 3346. The upper limit to the 408-MHz brightness using the Molonglo Radio Telescope is 30 mJy beam^{-1} (Harnett 1982).

NGC 3351. The peak and integrated flux densities at 20 cm with 54-arcsec resolution for the component associated with the galaxy are 34.8 mJy beam^{-1} and 45.3 mJy, respectively. There are confusing sources at RA $10^h41^m22^s.1$, Dec. 11°59′14″ and $10^h41^m23^s.9$, 11°55′49″ (Condon 1987). The northern source is resolved into two components in our image; the central feature has a ring-like structure and compact source towards the south-east.

NGC 3359. The VLA D-array image at 20 cm with a resolution of 60 arcsec has peak and total flux densities of 11.5 mJy beam^{-1} and 50.1 mJy, respectively (Condon 1987).

NGC 3504. The source has a large-scale halo which has been imaged by a number of authors (de Bruyn & Wilson 1976; Condon 1987; Gioia & Fabbiano 1987; Condon et al. 1990) besides the core component (Ulvestad, Wilson & Sramek 1981).

NGC 3627. The VLA D-array image at 20 cm (Condon 1987) and the 2.8-cm Effelsberg image (Urbanik, Gräve & Klein 1985) show two peaks of emission close to the end points of the bar where the spiral arms start. We detect a compact nuclear component between the two peaks, and weaker emission from the end points of the bar. The nuclear component has been quoted by Hummel et al. (1987) to have flux densities of 13 and 6 mJy at 2.7 and 8.1 GHz, respectively (Crane 1977). Comparison of our measurements with these values suggests that the compact component has a flat spectrum between 5 and 8 GHz.

NGC 4051. The VLA D- and C-array images at 20 cm have been published by Condon (1987) and Hummel et al. (1985). The component close to the nucleus is oriented east–west, with more extended emission towards the south-west. The nuclear component has been resolved by Ulvestad & Wilson (1984) into two components, separated by about 0.4 arcsec.

NGC 4064. WSRT observations by Kotanyi (1980) show that the flux density is 7 ± 2 mJy at 20 cm.

NGC 4124. Earlier attempts with coarser resolution have not detected radio emission from this galaxy (Wrobel 1991; Wrobel & Heeschen 1991).

NGC 4178, The VLA D-array image at 20 cm with a resolution of 54 arcsec shows that the radio image has two peaks of emission. The southern one, which is stronger, has a peak brightness of 5.9 mJy beam^{-1} and coincides with an optically bright knot at the south-western part of the galaxy (Condon 1987). The total flux density at 20 cm is 23.3 mJy.

NGC 4212. From VLA D-array observations at 20 cm,

Condon (1987) finds the source to be resolved along a PA of 76°, with peak and total flux densities of 11.9 mJy beam^{-1} and 23.7 mJy, respectively. Hummel et al. (1985) did not detect the source with the VLA C-array at 20 cm, and set an upper limit of 6 mJy for a central source less than about a kpc.

NGC 4258. There have been a large number of lower resolution studies of this galaxy with the WSRT at 20 (van Albada 1980) and 6 and 49 cm (de Bruyn 1977), the VLA C-array at 20 cm (Hummel et al. 1985), VLA D-array at 20 and 6 cm (Hummel, Krause & Lesch 1989), combined VLA and WSRT studies at 20 cm (van Albada & van der Hulst 1982), and at 2.8 and 6.3 cm with the Effelsberg telescope (Klein & Emerson 1981; Krause, Beck & Klein 1984). We detected a compact component close to the centre of the optical galaxy.

NGC 4303. The VLA D-array image at 20 cm shows the extended emission which has a peak brightness of 67.4 mJy beam^{-1} and a total flux density of 416 mJy (Condon 1987). A VLA 20-cm C-array image is shown in Condon (1983).

NGC 4314. The central source has a peak brightness of 11 mJy beam^{-1} at 20 cm with a resolution of 60 arcsec (Condon 1987; Gioia & Fabbiano 1987).

NGC 4394. A compact source with a peak brightness of 0.6 mJy beam^{-1} at 20 cm with a resolution of 54 arcsec was detected by Condon (1987). No nuclear component was detected by Hummel et al. (1987).

NGC 4457. The VLA D-array image at 20 cm with a resolution of 54 arcsec has peak and total flux densities of 23.9 mJy beam^{-1} and 37.4 mJy, respectively (Condon 1987). A 20-cm image of the central region with a resolution of about 1.3 arcsec shows a compact component with a flux density of 7.2 ± 0.3 mJy (Hummel et al. 1987). Comparison with our observations suggests that this feature has a steep spectrum with $\alpha \sim 0.8$.

NGC 5236. Low-resolution images of this galaxy at 20 cm with the VLA D- and C-arrays (Condon 1983, 1987), at 843 MHz with MOST (Harnett 1984), at 20 cm with the VLA B- and C-arrays, and at 6 cm with the C-array (Ondrechen 1985) show the emission from the bar and the disc of the galaxy. An A-array 20-cm image by Condon et al. (1982) shows the dominant emission from the central region. Our 6-cm image shows a number of significant peaks of emission in the central region.

NGC 5248. The VLA D-array image with 54-arcsec resolution shows a peak brightness of 48.9 mJy beam^{-1} and a total flux density of 140 mJy (Condon 1987). The radio emission from the galaxy as well as the strong confusing source to the north is seen in the VLA D- and C-array images (Hummel et al. 1985). We did not detect any radio emission from the galaxy, and we resolved the northern component into a triple source with a possible central component.

NGC 5253. The peak and total flux densities of the source at 20 cm with a resolution of 54 arcsec are 71.9 mJy beam^{-1} and 83.8 mJy, respectively (Condon 1987). We see a compact component surrounded by a larger scale halo and a secondary peak of emission.

NGC 5383. The VLA 20-cm image with a resolution of 15 arcsec shows a dominant component with peak and total flux densities of 10.7 mJy beam^{-1} and 30.4 mJy, respectively, and radio extensions which lie at the end of the optically bright bar (Condon et al. 1990). These features are also seen in the WSRT image at 1415 MHz (Sancisi & Ekers 1978).

NGC 5430. Condon et al. (1990) have presented VLA observations at 20 cm with resolutions of 15 and 5 arcsec. We resolve the dominant component into a spiral-like structure with several knots of emission. We also detect a compact feature in the southern component.

NGC 5597. VLA images with resolutions of 21 and 7 arcsec have peak brightnesses of 20.0 and 11.6 mJy beam^{-1}, respectively (Condon et al. 1990). We also detected weak emission from the nuclear region. There is a compact, unrelated source to the south-west which is listed in the table but not shown in the contour plot.

NGC 6217. VLA D-array image at 20 cm has peak and total flux densities of 61.4 mJy beam^{-1} and 78.4 mJy, respectively (Condon 1987). Higher resolution images with the VLA C- and B-arrays have been published by Hummel et al. (1985) and Condon et al. (1990). Higher resolution observations have been reported earlier by Hummel, van der Hulst & Dickey (1984) and Vila et al. (1990).

NGC 6951. Comparison of our image with the VLA C-array 20-cm image by Hummel et al. (1985) shows that the central component is resolved into a spiral-like pattern.

NGC 7741. The VLA 20-cm image with a resolution of 60 arcsec has peak and total flux densities of 4.9 mJy beam^{-1} and 13.3 mJy, respectively (Condon 1987). A 20-cm D-array image has been published by Gioia & Fabbiano (1987). Hummel et al. (1987) report an upper limit of 2 mJy at 20 cm for a nuclear component from observations with a resolution of about 1.3 arcsec.

5 DISCUSSION AND CONCLUDING REMARKS

With a median angular resolution of about 1.5 arcsec, which corresponds to a linear resolution of about 110 pc at a distance of 15 Mpc, we detected radio emission from 27 of the 47 galaxies observed. In Fig. 2, we show the distribution of distances for the galaxies with different types of optical nuclear structure, shading those for which radio emission has been detected. Those with prominent hotspots in the central regions (class σ and $\sigma\iota$) are almost always detected as radio sources, while only one of the five galaxies with very weak nuclei and no well-defined hotspots (class ι) was detected. For the other categories, the detection of radio emission bears no relation to the optical nuclear structure. In this sample of sources, the detection of radio emission from the nuclear regions also shows no significant dependence on whether the galaxy has been classified as a barred spiral.

The compact radio sources observed in these galaxies could be due to active galactic nuclei, bursts of star formation or a combination of both. The compact radio sources associated with the nuclei of active galaxies remain optically thin until synchrotron self-absorption sets in at brightness temperature $T_b \sim 10^{10}$ K, while those produced by a burst of star formation have $T_b < 10^5$ K. The compact sources seen in starburst galaxies could be either supernova remnants (SNRs) or regions of ionized hydrogen which become optically thick when T_b significantly exceeds the electron temperature. Using the peak brightness of the components and assuming their sizes to be similar to the

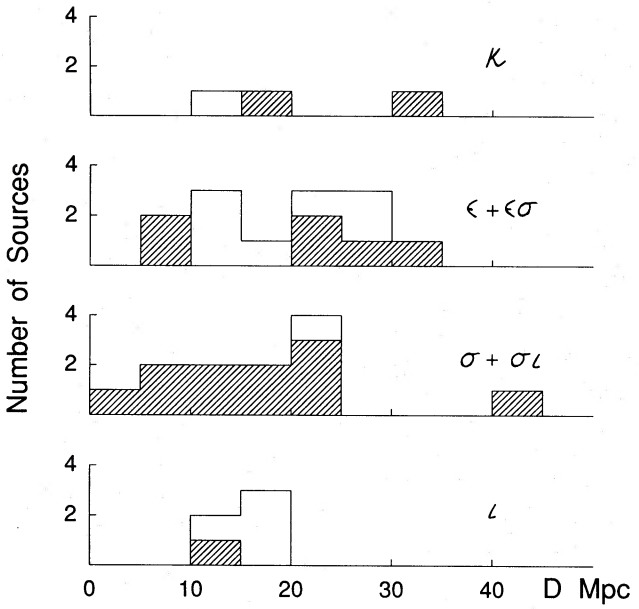

Figure 2. The distributions of the distances of the galaxies with different nuclear structure. Those detected as radio sources in our observations have been shaded.

resolution of our observations, we find the brightness temperatures to be invariably less than the limit of about 10^5 K. This is consistent with the bulk of them being either SNRs or regions of ionized hydrogen. The steep spectra of the individual peaks of emission for which we could determine the spectral indices, as well as the steep spectra of the regions of emission we detect, suggest that most of the components are likely to be SNRs.

To identify any possible AGN in our sample, one needs further tests. In the case of sources that are dominated by a nuclear component, one might be able to identify an AGN by looking for departures from the correlation between infrared and radio luminosities. However, for the weak AGN embedded in a starburst galaxy, this may not prove to be very useful. We have attempted to list the relatively weak AGN candidates by examining their spectra, luminosities and relative locations in the galaxies. The sources in our sample which show evidence of a relatively flat-spectrum component which might be due to an AGN are NGC 1140, 1300, 2196 and 3627. NGC 1300 shows evidence of a triple structure with the central component having a flat spectrum, while in NGC 2196 the compact southern component has a flat spectrum with $\alpha \sim 0.1$. NGC 2196 is one of the four sources in our sample whose components have luminosities $\log P \geq 20.5$ W Hz^{-1} at 6 cm. The other three are NGC 613, 2782 and 3504. Of these, NGC 613 has been shown to have a weak nuclear component by Hummel & Jörsäter (1992), while NGC 2782 and 3504 have dominant compact components surrounded by more diffuse extended emission. The luminosities of these compact features overlap with the lower end of the luminosity distribution of the compact components seen in the nuclear regions of Seyfert galaxies (Kukula et al., in preparation).

In Fig. 3, we present the luminosity distributions of all the components we see in our images, using their peak brightnesses and the distances listed in Table 1. The median values of $\log P$ are about 19.8 and 19.7 W Hz^{-1} at 20 and 6 cm, respectively. For comparison, we also show the distributions of the luminosities for the 23 brightest SNRs in M82, using the flux densities from recent MERLIN observations at 5 GHz and assuming a distance of 3.2 Mpc (Muxlow et al. 1994), and also for the 22 SNRs in our Galaxy for which we have reliable distances (Milne 1979). The median values of $\log P$ for these distributions are 18.25 and 17.1 W Hz^{-1}, respectively. If it is assumed that the bulk of the compact sources we detect in our sample are likely to be SNRs, they appear to be more luminous than those in M82 and in our own Galaxy. This is perhaps not surprising, since we are sampling only the brightest and possibly the youngest remnants in these relatively distant galaxies, with the weaker ones being below our detection limits. Some of the difference, however, could also be due to the relatively coarse resolution of the observations, which may include the contribution of several remnants and some of the more extended emission within the restoring beam. Higher resolution observations would enable us to determine their flux densities and brightness temperatures more accurately.

A number of images in our sample show evidence of ring or spiral-like structures in the nuclear regions. Nuclear rings are small rings often found in the central regions of early-type barred and oval disc galaxies. They are rich in gas and stars, and form an important aspect of our understanding of the dynamics of gas and star-formation processes in the nuclear regions (cf. Buta & Crocker 1993, and references therein). These rings could be due to a strong bar which causes these structures to form at the inner Lindblad resonance (Gerin, Nakai & Combes 1988), or could be due to viscous outward transport of angular momentum (Icke 1979; Lesch et al. 1990). There is an enhancement of gas density and star formation which leads to increased emission at different wavebands including radio continuum emission. In our sample of sources, the rings in NGC 613 and 1365 are well known and have been studied at radio wavelengths (Hummel & Jörsäter 1992; Sandqvist et al. 1982, 1994 in preparation). We find evidence of weak radio rings in three more galaxies, namely NGC 1530, 2997 and 3351, and the radio continuum emission resembles nuclear spiral arms in NGC 5430 and 6951. Such structures could be due to the ejection of plasma from a rotating nucleus in opposite directions (Pişmis & Moreno 1987), or the development of an instability in the core due to tidal interactions (Subramanian 1989). Each of these galaxies has a compact component in the centre of the spiral-like structure. Higher resolution, multifrequency observations would help to clarify whether there is an active nucleus with jets of radio-emitting material in opposite directions.

ACKNOWLEDGMENTS

We thank the staff of the National Radio Astronomy Observatory for help with the observations. The National Radio Astronomy Observatory is operated by Associated Universities, Inc. under co-operative agreement with the National Science Foundation. We thank Jacqueline van Gorkom for her help and advice with the first set of observations, Jim Cohen, Rod Davies and Graham Smith for their comments on the manuscript, Sandy Sandqvist for communicating the results on NGC 1365 prior to publication, and

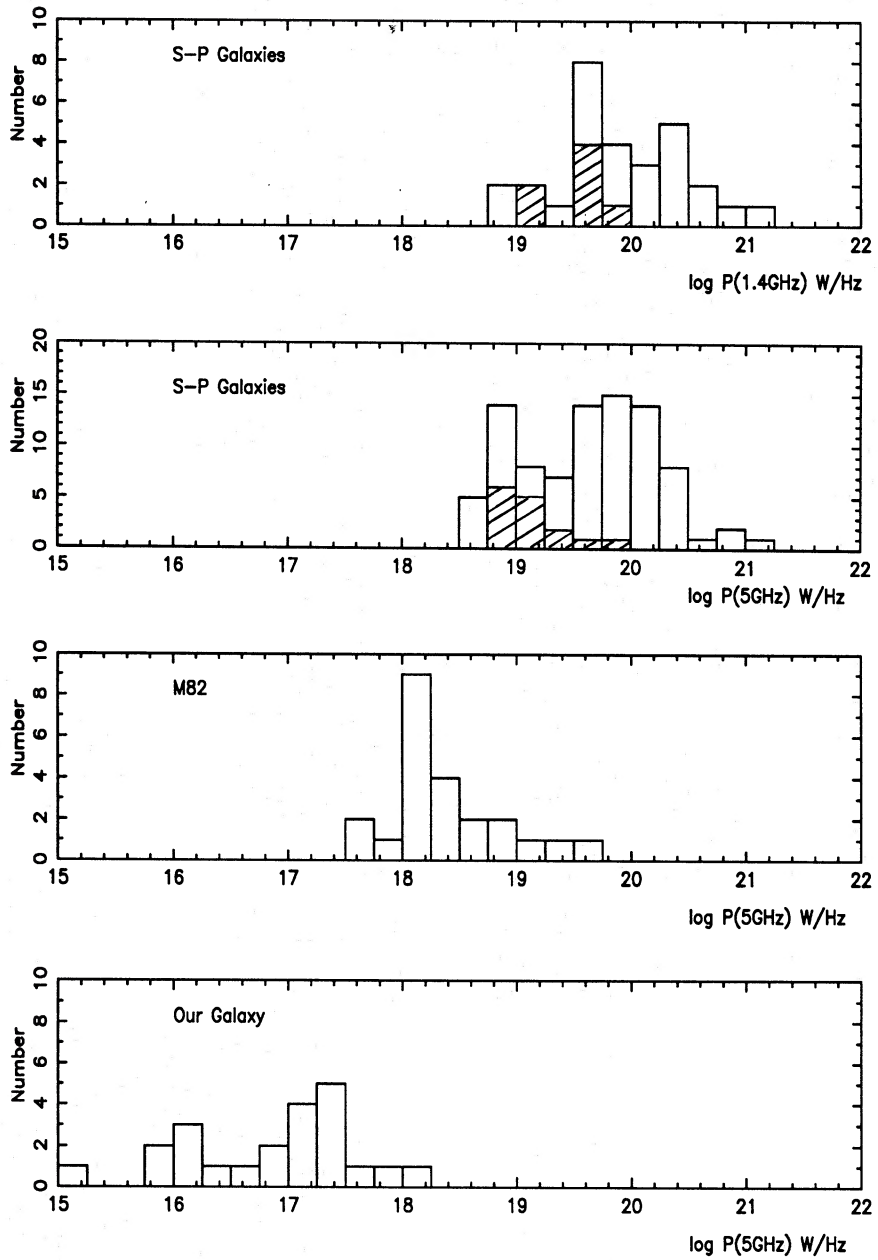

Figure 3. The distributions of the luminosities of the compact components in the Sérsic–Pastoriza galaxies at 20 and 6 cm, and of the SNRs in M82 and in our Galaxy at 6 cm. Upper limits for galaxies without any detected compact components are shown shaded.

Graham Yates for his assistance with the project. This research has made use of the NASA/IPAC Extragalactic Database (NED), which is operated by the Jet Propulsion Laboratory, Caltech, under contract with the National Aeronautics and Space Administration. DJS thanks the Director, Jodrell Bank, for hospitality and support during the course of this work.

REFERENCES

Baars J. W. M., Genzel R., Pauliny-Toth I. I. K., Witzel A., 1977, A&A, 61, 99
Balick B., Heckman T., 1981, A&A, 96, 271
Buta R., Crocker D. A., 1993, AJ, 105, 1344
Carral P., Turner J. L., Ho P. T. P., 1990, ApJ, 362, 434
Colina L., Pérez-Olea D., 1992, MNRAS, 259, 709
Condon J. J., 1983, ApJS, 53, 459
Condon J. J., 1987, ApJS, 65, 485
Condon J. J., Condon M. A., Gisler G., Puschell J. J., 1982, ApJ, 252, 102
Condon J. J., Helou G., Sanders D. B., Soifer B. T., 1990, ApJS, 73, 359
Condon J. J., Huang Z.-P., Yin Q. F., Thuan T. X., 1991, ApJ, 378, 65
Crane P. C., 1977, PhD thesis, Massachusetts Institute of Technology
de Bruyn A. G., 1977, A&A, 58, 221
de Bruyn A. G., Wilson A. S., 1976, A&A, 53, 93
de Vaucouleurs G., de Vaucouleurs A., Corwin H. G., Jr, Buta R. J., Paturel G., Fouqué P., 1991, Third Reference Catalogue of Bright Galaxies. Springer-Verlag, Berlin
Duric N., Seaquist E. R., Crane P. C., Davis L. E., 1986, ApJ, 304, 82

Gerin M., Nakai N., Combes F., 1988, A&A, 203, 44
Gioia I. M., Fabbiano G., 1987, ApJS, 63, 771
Harnett J. I., 1982, Aust. J. Phys., 35, 321
Harnett J. I., 1984, MNRAS, 210, 13
Harnett J. I., 1987, MNRAS, 227, 887
Heckman T. M., 1990, in Sulentic J., Keel W., Telesco C., eds, NASA CP3098, Paired and Interacting Galaxies. p. 359
Heckman T. M., 1991, in Leitherer C., Walborn N., Heckman T., Norman C., eds, Massive Stars in Starburst Galaxies. Cambridge Univ. Press, Cambridge, p. 289
Heckman T. M., 1992, in Holt S. S., Neff S. G., Urry C. M., eds, AIP Conf. Proc. 254, Testing the AGN Paradigm. American Institute of Physics, New York, p. 595
Helou G., Soifer B. T., Rowan-Robinson M., 1985, ApJ, 298, L7
Helou G., Madore B. F., Schmitz M., Bicay M. D., Wu X., Bennett J., 1991, in Egret D., Albrecht M., eds, Databases and On-Line Data in Astronomy. Kluwer, Dordrecht, p. 89
Hummel E., Jörsäter S., 1992, A&A, 261, 85
Hummel E., van der Hulst J. M., Dickey J. M., 1984, A&A, 134, 207
Hummel E., Pedlar A., van der Hulst J. M., Davies R. D., 1985, A&AS, 60, 293
Hummel E., van der Hulst J. M., Keel W. C., Kennicutt R. C., Jr, 1987, A&AS, 70, 517
Hummel E., Krause M., Lesch H., 1989, A&A, 211, 266
Icke V., 1979, A&A, 78, 21
Klein U., Emerson D. T., 1981, A&A, 94, 29
Kotanyi C. G., 1980, A&AS, 41, 421
Krause M., Beck R., Klein U., 1984, A&A, 138, 385
Kronberg P. P., Biermann P., 1981, ApJ, 243, 89
Kukula M. J., Ghosh T., Pedlar A., Schilizzi R. T., Miley G. K., de Bruyn A. G., Saikia D. J., 1993 MNRAS, 264, 893
Lauberts A., 1982, The ESO/Uppsala Survey of the ESO (B) Atlas, ESO, Garching
Lesch H., Biermann P. L., Crusius A., Reuter H. P., Dahlem M., Barteldrees A., Wielebinski R., 1990, MNRAS, 242, 194
Milne D. K., 1979, Aust. J. Phys., 32, 83
Muxlow T. W. B., Pedlar A., Wilkinson P. N., Axon D. J., Sanders E. M., de Bruyn A. G., 1994, MNRAS, 266, 455
Neff S. G., Hutchings J. B., 1992, AJ, 103, 1746
Neff S. G., Ulvestad J. S., 1988, AJ, 96, 841
Nilson P., 1973, Uppsala General Catalogue of Galaxies, Uppsala Astronomical Observatory
Norman C., Scoville N., 1988, ApJ, 332, 124
Norris R. P., Allen D. A., Sramek R. A., Kesteven M. J., Troup E. R., 1990, ApJ, 359, 291
Ondrechen M. P., 1985, AJ, 90, 1474
Osmer P. S., Smith M. G., Weedman D. W., 1974, ApJ, 192, 279
Pişmis P., Moreno E., 1987, in Khachikian E. Ye., ed., Proc. IAU Symp. 121, Observational Evidence of Activity in Galaxies. Reidel, Dordrecht, p. 477
Prabhu T. P., 1980, JA&A, 1, 129
Saikia D. J., Unger S. W., Pedlar A. P., Yates G., Axon D. J., Wolstencroft R. D., Taylor K., Gyldenkerne K., 1990, MNRAS, 245, 397
Sancisi R., Ekers R. D., 1978, A&A, 67, L21
Sandage A., Tammann G. A., 1981, A Revised Shapley–Ames Catalog of Bright Galaxies, Carnegie Institution of Washington
Sandqvist A., Jörsäter S., Lindblad P. O., 1982, A&A, 110, 336
Sérsic J. L., 1973, PASP, 85, 103
Sérsic J. L., Pastoriza M., 1965, PASP, 77, 287
Sopp H. M., Alexander P., 1991, MNRAS, 251, 112
Subramanian K., 1989, MNRAS, 238, 1345
Ulvestad J. S., Wilson A. S., 1984, ApJ, 285, 439
Ulvestad J. S., Wilson A. S., Sramek R. A., 1981, ApJ, 247, 419
Urbanik M., Gräve R., Klein U., 1985, A&A, 152, 291
van Albada G. D., 1980, A&AS, 39, 283
van Albada G. D., van der Hulst J. M., 1982, A&A, 115, 263
van der Hulst J. M., Crane P. C., Keel W. C., 1981, AJ, 86, 1175
van der Kruit P. C., 1973, A&A, 29, 231
van der Kruit P. C., de Bruyn A. G., 1976, A&A, 48, 373
Vila M. B., Pedlar A., Davies R. D., Hummel E., Axon D. J., 1990, MNRAS, 242, 379
Weedman D. W., 1983, ApJ, 266, 479
Wilson A. S., Willis A. G., 1980, ApJ, 240, 429
Wrobel J. M., 1991, AJ, 101, 127
Wrobel J. M., Heeschen D. S., 1991, AJ, 101, 148
Wynn-Williams C. G., Becklin E. E., 1985, ApJ, 290, 108